Title

Deuterium magnetic resonance spectroscopy enables noninvasive metabolic imaging of tumor burden and response to therapy in low-grade gliomas



Journal

Neuro-Oncology, 24(7)

ISSN

1522-8517

Authors

Taglang, Céline
Batsios, Georgios
Mukherjee, Joydeep
et al.

Publication Date

2022-07-01

DOI

10.1093/neuonc/noac022

Peer reviewed

Neuro-Oncology

24(7), 1101–1112, 2022 | https://doi.org/10.1093/neuonc/noac022 | Advance Access date 29 January 2022

# Deuterium magnetic resonance spectroscopy enables noninvasive metabolic imaging of tumor burden and response to therapy in low-grade gliomas

**Céline Taglang, Georgios Batsios, Joydeep Mukherjee, Meryssa Tran, Anne Marie Gillespie, Donghyun Hong, Sabrina M. Ronen, Hema Artee Luchman, Russell O. Pieper, and Pavithra Viswanath**

*Department of Radiology and Biomedical Imaging, University of California, San Francisco, San Francisco, California, USA (C.T., G.B., M.T., A.M.G., D.H., S.M.R., P.V.); Department of Neurological Surgery, University of California, San Francisco, San Francisco, California, USA (J.M., R.O.P.); Department of Cell Biology and Anatomy, Hotchkiss Brain Institute and Arnie Charbonneau Cancer Institute, University of Calgary, Calgary, Alberta, Canada (H.A.L.)*

**Corresponding Author:** Pavithra Viswanath, PhD, Department of Radiology and Biomedical Imaging, University of California, San Francisco, 1700 4th St, San Francisco, CA 94143, USA (pavithra.viswanath@ucsf.edu).

**Abstract**

**Background.** The alternative lengthening of telomeres (ALT) pathway is essential for tumor proliferation in astrocytomas. The goal of this study was to identify metabolic alterations linked to the ALT pathway that can be exploited for noninvasive magnetic resonance spectroscopy (MRS)-based imaging of astrocytomas in vivo.

**Methods.** Genetic and pharmacological methods were used to dissect the association between the ALT pathway and glucose metabolism in genetically engineered and patient-derived astrocytoma models. $^{2}$H-MRS was used for noninvasive imaging of ALT-linked modulation of glycolytic flux in mice bearing orthotopic astrocytomas in vivo.

**Results.** The ALT pathway was associated with higher activity of the rate-limiting glycolytic enzyme phosphofructokinase-1 and concomitantly elevated flux of glucose to lactate in astrocytoma cells. Silencing the ALT pathway or treating with the poly(ADP-ribose) polymerase inhibitor niraparib that induces telomeric fusion in ALT-dependent astrocytoma cells abrogated glycolytic flux. Importantly, this metabolic reprogramming could be non-invasively visualized by $^{2}$H-MRS. Lactate production from [6,6′-$^{2}$H]-glucose was higher in ALT-dependent astrocytoma tumors relative to the normal brain in vivo. Furthermore, treatment of orthotopic astrocytoma-bearing mice with niraparib reduced lactate production from [6,6′-$^{2}$H]-glucose at early timepoints when alterations in tumor volume could not be detected by anatomical imaging, pointing to the ability of [6,6′-$^{2}$H]-glucose to report on pseudoprogression in vivo.

**Conclusions.** We have mechanistically linked the ALT pathway to elevated glycolytic flux and demonstrated the ability of [6,6′-$^{2}$H]-glucose to non-invasively assess tumor burden and response to therapy in astrocytomas. Our findings point to a novel, clinically translatable method for metabolic imaging of astrocytoma patients.

## Key Points

- The ALT pathway increases glycolytic flux in astrocytomas via elevated activity of the rate-limiting glycolytic enzyme phosphofructokinase-1.
- Deuterium MRS-based imaging of ALT status can report on tumor burden and response to therapy in astrocytomas in vivo.

## Importance of the Study

Glioma patient management is heavily dependent on MRI. However, astrocytomas can be difficult to visualize by MRI and, importantly, MRI does not reliably distinguish tumor progression from pseudoprogression. In this study, we show that metabolic reprogramming associated with telomere maintenance via the ALT pathway, which is a fundamental hallmark of tumor proliferation, can be leveraged for astrocytoma imaging in vivo. Our results indicate that the ALT pathway is associated with enhanced glycolytic flux, an effect that can be non-invasively visualized using [6,6′-$^2$H]-glucose in mice bearing orthotopic astrocytomas in vivo. Importantly, [6,6′-$^2$H]-glucose reports on response to therapy at early timepoints that precede MRI-detectable alterations in tumor volume, suggesting that [6,6′-$^2$H]-glucose can assess pseudoprogression in vivo. Collectively, our study identifies deuterium metabolic imaging following administration of [6,6′-$^2$H]-glucose as a novel method of imaging the ALT pathway that has the potential to improve tumor imaging and treatment response assessment for astrocytoma patients.

Telomeres are cap-like structures that protect the ends of linear chromosomes from damage.[1] Cell proliferation is accompanied by telomere shortening and, therefore, cancer cells need a mechanism of maintaining telomere length to sustain uncontrolled proliferation.[1] ~85% of human tumors maintain telomeres via reactivation of the expression of telomerase reverse transcriptase.[1] However, ~15% of tumors, including mutant isocitrate dehydrogenase (IDHmut)-positive astrocytomas, utilize the alternative lengthening of telomeres (ALT) pathway, which is a telomerase-independent, homologous recombination-based method of telomere maintenance.[2] Loss-of-function mutations in the tumor suppressor gene alpha-thalassemia/mental retardation syndrome X-linked (*ATRX*) are necessary for activation of the ALT pathway[3–5] and ATRX re-expression in astrocytoma cells abrogates the ALT pathway.[6–8] ATRX is a chromatin remodeling protein that maintains genome stability by regulating deposition of the histone variant H3.3 at telomeres and pericentric heterochromatin.[9]

Assessment of ALT status has diagnostic, prognostic, and therapeutic significance for glioma patients. According to 2021 WHO guidelines, the occurrence of ATRX mutations is a diagnostic feature of IDHmut astrocytomas, which have been recognized as a distinct entity for the first time.[10] In contrast, IDHmut tumors that are ATRX-positive and carry 1p/19q codeletions are classified as oligodendroglioma, IDHmut[10] and these tumors maintain telomeres via telomerase reverse transcriptase.[1,5] Although the full prognostic significance of ATRX mutations and the ALT pathway remains to be determined, astrocytomas patients have worser prognosis compared to oligodendroglioma patients.[8,11,12] From a therapeutic perspective, targeting the ALT pathway is promising since ALT is not used by normal cells and is critical for tumor proliferation.[2,13–15]The ATR kinase inhibitor berzosertib and poly(ADP-ribose) polymerase inhibitors (PARPi) such as olaparib and niraparib inhibit proliferation of ALT tumors, including astrocytomas.[13–16] Importantly, while PARPi cause DNA damage in a variety of tumors,[17] cells using the ALT mechanism undergo telomeric fusion-mediated cell death, rendering them hypersensitive to PARPi, which are in clinical trials for astrocytoma patients.[13,16,17]

Currently, the ALT status of tumors is inferred from phenotypic features of the ALT pathway. Since ATRX mutations are widely considered a surrogate marker for the ALT phenotype,[3–5] assessment of ALT status can be done via immunohistochemical detection of ATRX loss.[12] Robust, quantitative detection of the ALT pathway can also be achieved via PCR-based assays for extra-chromosomal telomeric repeats known as c-circles that are exclusively present in ALT cells.[18,19] Another method is quantification of ALT-associated promyelocytic leukemia nuclear bodies by telomeric fluorescence in situ hybridization.[2,18,19] However, these methods are invasive, which precludes longitudinal assessment of ALT status in glioma patients wherein the anatomical location of the tumor restricts repeated biopsy sampling.

Magnetic resonance spectroscopy (MRS) is a noninvasive, non-radioactive method of imaging metabolism.[20]Thermally polarized $^{13}$C-MRS following administration of $^{13}$C-labeled substrates reports on specific metabolic pathways,[20] but its low sensitivity has hindered clinical application.[21]The advent of hyperpolarized $^{13}$C-MRS has improved the signal-to-noise ratio (SNR) and provided an in vivo, albeit technically demanding, method of assessing metabolic fluxes.[22] Recently, $^2$H-MRS following delivery of $^2$H-labeled substrates emerged as a novel, complementary, easy-to-implement method of imaging metabolic fluxes in vivo.[23] [6,6′-$^2$H]-glucose has been used to monitor flux to lactate in preclinical glioblastoma and lymphoma models[23,24] and to glx (sum of glutamate and glutamine, since these resonances cannot be resolved in vivo) in the normal brain.[23–25] Importantly, clinical studies indicate that [6,6′-$^2$H]-glucose can be used to visualize tumor burden in glioblastoma patients.[23]

Since the ALT pathway is intrinsically linked to tumor proliferation and is a therapeutic target, noninvasive methods of imaging ALT have the potential to report on tumor burden and treatment response in astrocytomas. We previously showed that the ALT pathway is associated with elevated hyperpolarized $^{13}$C-glucose flux to lactate in a genetically engineered astrocytoma model.[26] However, that study did not examine the mechanistic link between the ALT pathway and glycolysis nor did it assess clinically relevant astrocytoma models.[26] The goal of the current study was to mechanistically dissect the link between the ALT pathway and glucose metabolism in genetically engineered and patient-derived astrocytoma models and assess the utility of [6,6′-$^2$H]-glucose for noninvasive imaging of the ALT pathway. Our results indicate that the ALT pathway is associated with elevated activity of the rate-limiting glycolytic enzyme phosphofructokinase-1 (PFK1).

Importantly, we show that [6,6′-$^2$H]-glucose can be used to non-invasively visualize the ALT pathway and response to therapy in astrocytomas in vivo.

## Materials and Methods

Detailed experimental procedures are provided in the Supplementary material.

### Cell Models

Immortalized normal human astrocytes expressing IDHmut ($NHA_{CONTROL}$) have been previously described.[27] $NHA_{ALT}$ cells were generated by the knockout of ATRX in $NHA_{CONTROL}$ cells.[6] $NHA_{CONTROL}$ and $NHA_{ALT}$ cells produce similar levels of 2-hydroxyglutarate (2-HG, the product of the IDHmut enzyme; see reference[28] and Supplementary Figure S1A). BT142 and BT257 neurospheres were established from patients with IDHmut-positive, ATRX-deficient astrocytomas and grown in a serum-free medium.[29–31] The IDHmut status of these lines has been previously confirmed.[29–31] BT142 neurospheres lack 2-HG[29,30] while BT257 neurospheres produce 2-HG[31] (Supplementary Figure S1A and B). The ALT status of our models has been verified by confirming loss of ATRX and the presence of c-circles (as detailed in references[6,28] and Supplementary Figure S1C and D). c-circles were quantified by telomeric qPCR with and without amplification by φ29 polymerase.[2,28] Telomeric sister chromatid exchange, which is also a phenotypic hallmark of ALT, has previously been confirmed in these models.[16,27,28] ALT silencing was achieved by transiently restoring ATRX expression in BT142 and BT257 neurospheres by transfection with the plasmid IF-GFP-ATRX.[3,27,28] PFKP silencing was achieved by RNA interference using 2 non-overlapping siRNA pools (Dharmacon). For PFKP overexpression, BT257 neurospheres were first transfected with IF-GFP-ATRX followed by transfection with human PFKP (Genecopoeia). Pharmacological inhibition of ALT cells was achieved by treatment with niraparib (1 μM)[13,16] and verified by assessment of telomeric fusion by fluorescence in situ hybridization.[16] Cell lines were routinely tested for mycoplasma contamination, authenticated by fingerprinting, and assayed within 6 months.

### Neurosphere Assays

For assessment of viability, neurospheres were seeded at 1000 cells/well in 96-well plates, and viability was quantified at 14 days using a cytotoxicity kit (Abcam, ab112118).[32] For quantification of growth, the number of neurospheres/well was quantified after 21 days.[32]

### Chromatin Immunoprecipitation-Quantitative Reverse Transcription Polymerase Chain Reaction (ChIP-qRT-PCR)

ChIP was performed using a kit (Abcam) with antibodies against histone H3K27me3 and total histone H3. Rabbit IgG was used as isotype control. *PFKP* promoter fragments were amplified by qRT-PCR. Data were expressed as fold enrichment relative to IgG control.

### Patient Biopsies

Astrocytoma or non-neoplastic gliosis biopsies were obtained from the UCSF Brain Tumor Center Biorepository in compliance with the informed consent policy.[26,28,33,34]

### Gene Expression and Activity

PFK1 activity was measured using a kit (Abcam). *PFKP* (platelet-specific isoform of PFK) and *ATRX* expression was assessed by qRT-PCR.

### MRS of Cell Extracts

Metabolites were extracted by methanol-chloroform extraction.[26,33,34] For $^{13}$C-MRS, cells were cultured in a medium containing 5 mM [1-$^{13}$C]-glucose for 48 hours. $^1$H- and $^{13}$C-MR spectra were obtained using a 11.7T spectrometer. Peak integrals were quantified and normalized to an external reference and to cell number.[26,33,34]

### MRI

Animal studies were conducted in accordance with UCSF Institutional Animal Care and Use Committee guidelines. $NHA_{ALT}$ or BT257 cells were intracranially injected into female SCID mice.[33,34] Tumor volume was determined by T2-weighted MRI using a 14.1T scanner and a spin-echo multi-slice sequence.[33,34] Once tumors were ~20 mm$^3$, animals were randomized and treated with vehicle-control (saline) or niraparib (100 mg/kg for the BT257 model and 200 mg/kg for $NHA_{ALT}$) daily via intraperitoneal injection.[16] Animal survival was assessed by Kaplan-Meier analysis.

### $^2$H-MRS In Vivo

Studies were performed on a 14.1T spectrometer using a 16 mm $^2$H surface coil. Following intravenous injection of a bolus of [6,6′-$^2$H]-glucose (1 g/kg), non-localized $^2$H-MR spectra were acquired. Metabolites were referenced to semi-heavy water (HDO; 4.75 ppm). Absolute concentrations were determined by correcting peak integrals for number of deuterons, saturation and normalizing to pre-injection HDO (estimated to be 10.12 mM[23–25]). Since [6,6′-$^2$H]-glucose metabolism results in release of HDO (as evidenced by higher HDO in post-injection spectra relative to pre-injection, see Figure 4A), metabolite peak integrals were also normalized to peak integrals for [6,6′-$^2$H]-glucose, post-injection HDO and pre-injection HDO (henceforth referred to as normalized lactate) as described previously.[35] For spatial localization, a 2D chemical shift imaging (CSI) sequence was used. Data were analyzed in Matlab, and the SNR of lactate was calculated in voxels from the tumor and contralateral normal brain.

### Statistical Analysis

All experiments were performed on a minimum of 3 samples ($n \geq 3$), and results were presented as mean ± standard deviation. Statistical significance was assessed in GraphPad Prism 9 using a Welch's *t* test, ordinary 1-way or 2-way ANOVA with $P < .05$ considered significant. Analyses were corrected for multiple comparisons using Tukey's method, wherever applicable. $*P < .05$, $**P < .01$, $***P < .005$, $****P < .0001$, ns, not significant.

## Results

### The ALT Pathway Is Associated With Higher Glycolytic Flux in Astrocytoma Cells

We examined IDHmut-expressing normal human astrocytes that have been immortalized via knockdown of p53 and pRb and genetically engineered to use the ALT pathway via CRISPR-mediated knockout of ATRX ($NHA_{ALT}$).[6,16,26–28] $NHA_{ALT}$ cells serve as a model of astrocytomas which are characterized by the presence of IDHmut and loss of ATRX and p53.[10] As controls, we examined isogenic cells that retain ATRX and lack a telomere maintenance mechanism ($NHA_{CONTROL}$).[6,26–28] The ALT status of these cell lines has previously been verified by quantification of c-circles, ALT-associated promyelocytic leukemia nuclear bodies, and telomere sister chromatid exchange.[6,16,26,28] Here, we confirmed loss of ATRX and the presence of c-circles in $NHA_{ALT}$ cells relative to $NHA_{CONTROL}$ (Supplementary Figure S1C and D).

Thermally polarized $^{13}$C-MRS is the gold standard for measuring glycolytic flux.[20,21] Following incubation with [1-$^{13}$C]-glucose, [3-$^{13}$C]-lactate production was significantly higher in $NHA_{ALT}$ cells relative to $NHA_{CONTROL}$ (Figure 1A and B). Importantly, elevated glycolytic flux was associated with the ALT pathway in clinically relevant

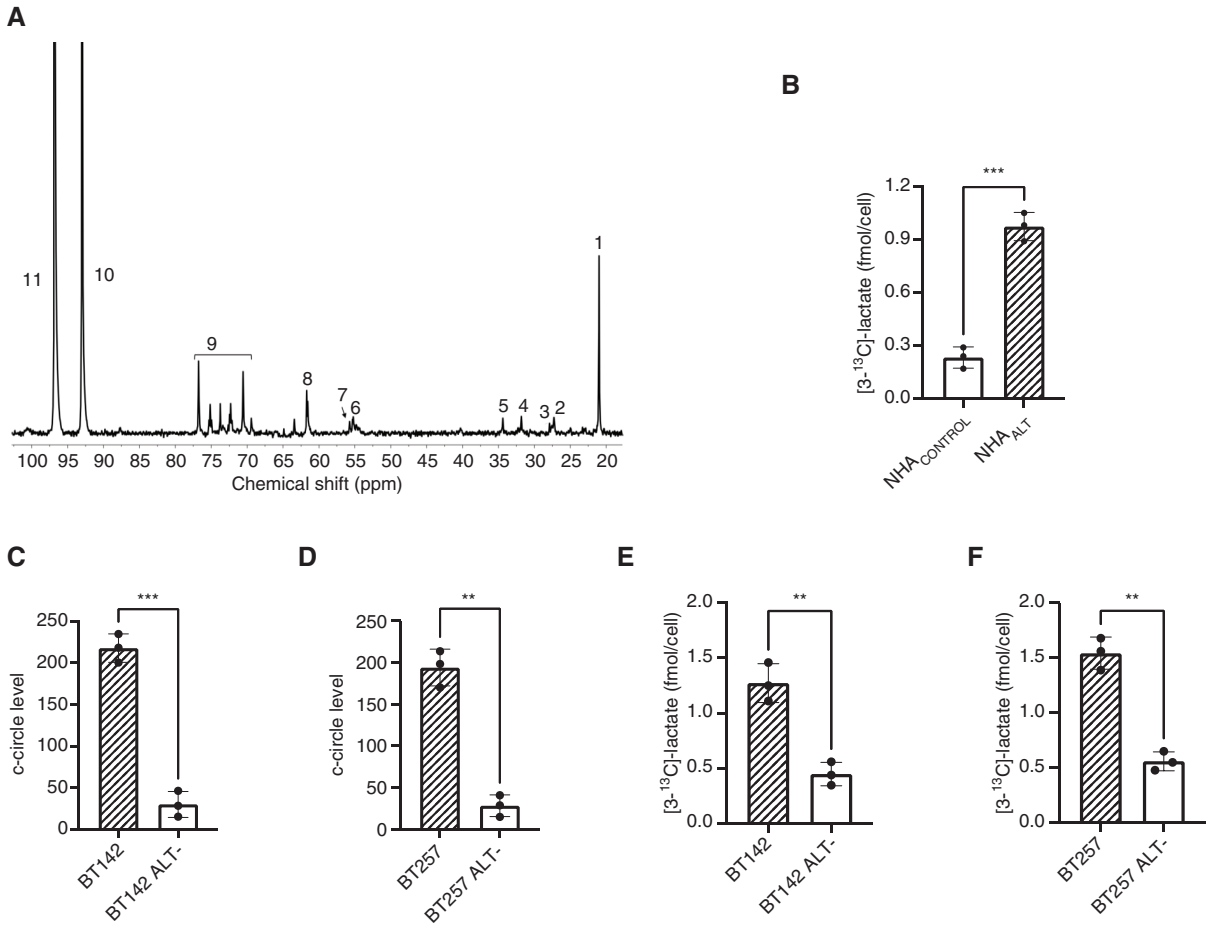


**Fig. 1** The ALT pathway is associated with elevated glycolytic flux in astrocytoma cells. (A) Representative $^{13}$C-MR spectrum from $NHA_{ALT}$ cells incubated with [1-$^{13}$C]-glucose. Peaks correspond to 1 = [3-$^{13}$C]-lactate; 2 = [3-$^{13}$C]-glutamine; 3 = [3-$^{13}$C]-glutamate; 4 = [4-$^{13}$C]-glutamine; 5 = [4-$^{13}$C]-glutamate; 6 = [5-$^{13}$C]-glutamine; 7 = [5-$^{13}$C]-glutamate; 8 = [6-$^{13}$C]-glucose; 9 = [2-$^{13}$C]-glucose, [3-$^{13}$C]-glucose, [4-$^{13}$C]-glucose, [5-$^{13}$C]-glucose; 10 = α-[1-$^{13}$C]-glucose; 11 = β-[1-$^{13}$C]-glucose. (B) [3-$^{13}$C]-lactate in $NHA_{CONTROL}$ and $NHA_{ALT}$ cells. Effect of ALT silencing on c-circles in the BT142 (C) and BT257 (D) models. Effect of ALT silencing on [3-$^{13}$C]-lactate production in the BT142 (E) and BT257 (F) models. Statistical significance was assessed using a Welch's *t* test with $P < .05$ considered significant. $**P < .01$, $***P < .005$.

patient-derived astrocytoma models. We silenced the ALT pathway in BT142 and BT257 neurospheres by transient re-expression of ATRX (Supplementary Figure S2A and B) as described previously.[6,28] We previously confirmed that ATRX re-expression results in loss of ALT-associated telomere sister chromatid exchange in these models.[6,28] Here, we verified inhibition of the ALT pathway in BT142 ALT- and BT257 ALT- neurospheres by confirming loss of c-circles (Figure 1C and D). ALT silencing did not significantly alter growth or neurosphere formation (Supplementary Figure S2C–F), consistent with prior studies indicating that ALT silencing via ATRX re-expression does not induce pronounced growth defects.[4,6] In line with these results, ALT silencing did not alter levels of phosphocholine, an intermediate in phospholipid biosynthesis which is considered a marker of tumor proliferation[36] (Supplementary Figure S2G and H). Importantly, ALT silencing significantly reduced [3-$^{13}$C]-lactate production from [1-$^{13}$C]-glucose in BT142 and BT257 neurospheres (Figure 1E and F). Collectively, these results point to a causal link between the ALT pathway and glycolysis in astrocytomas.

## ALT-Linked Increase in Glycolytic Flux in Astrocytoma Cells Is Mediated via PFK

PFK1 catalyzes the irreversible conversion of fructose-6-phosphate to fructose-1,6-bisphosphate, which is the first committed and rate-limiting step in glycolysis[37] (see schematic in Figure 2A). PFKP is the predominant PFK1 isoform in the brain and its expression is upregulated in many cancers, including gliomas.[38] PFKP expression (Supplementary Figure S3A) and activity (Figure 2B) were significantly elevated in $NHA_{ALT}$ cells relative to $NHA_{CONTROL}$. Silencing ALT significantly reduced PFKP expression (Supplementary Figure S3B and C) and PFK activity (Figure 2C and D) in BT142 and BT257 neurospheres. Importantly, silencing PFKP (Supplementary Figure S3D and E) significantly reduced [3-$^{13}$C]-lactate production from [1-$^{13}$C]-glucose in BT257 neurospheres (Figure 2E). Conversely, PFKP overexpression in BT257 ALT- neurospheres (Supplementary Figure S3F and G) rescued the reduction in [3-$^{13}$C]-lactate production from [1-$^{13}$C]-glucose caused by ALT silencing (Figure 2F).

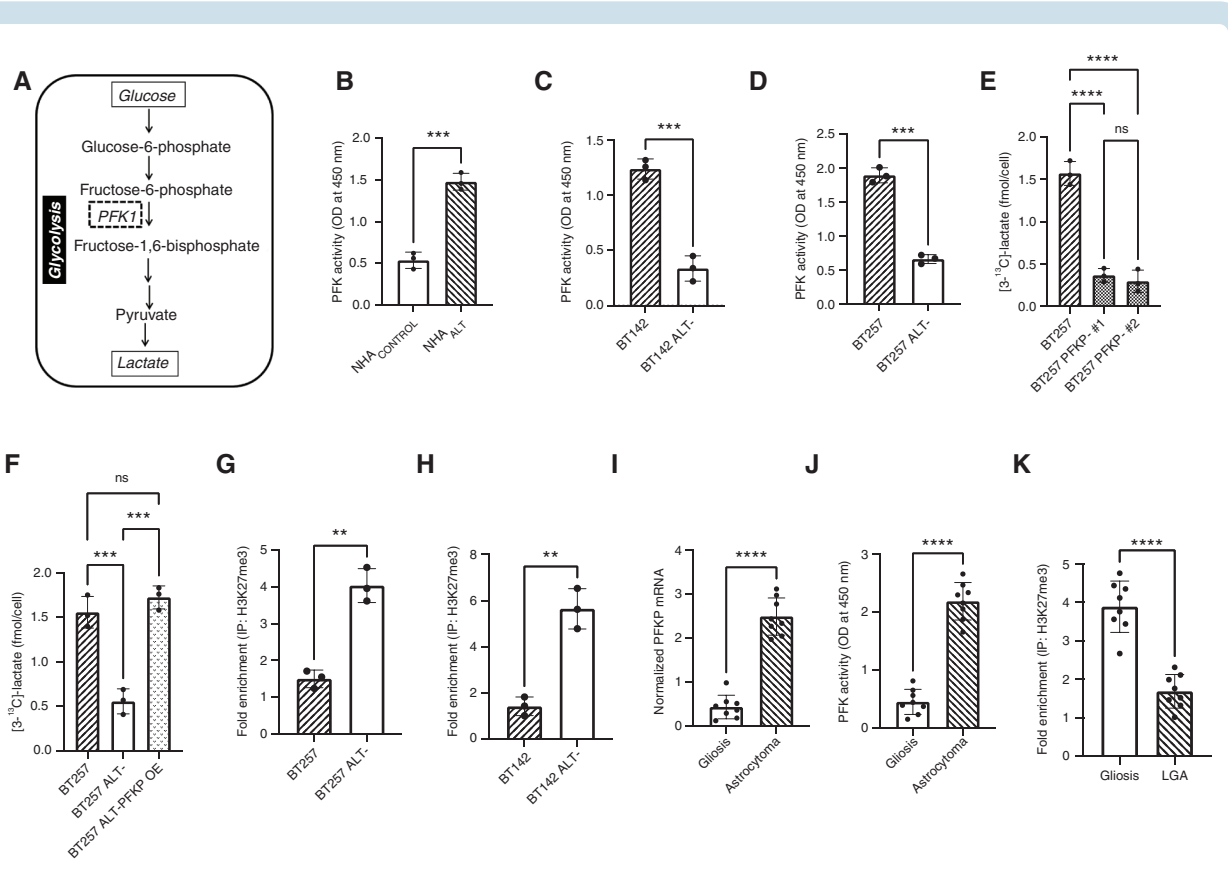


**Fig. 2** The ALT pathway is associated with elevated PFK activity in astrocytoma cells. (A) Schematic representation of glycolysis highlighting the role of PFK1. (B) PFK activity in $NHA_{CONTROL}$ and $NHA_{ALT}$ cells. Effect of ALT silencing on PFK activity in the BT142 (C) and BT257 (D) models. Effect of PFKP silencing (E) or PFKP overexpression (F) on [3-$^{13}$C]-lactate production from [1-$^{13}$C]-glucose in the BT257 model. ChIP-qRT-PCR of the *PFKP* promoter using an antibody against histone H3K27me3 in the BT257 (G) and BT142 (H) models. PFKP mRNA (I), PFK activity (J), and histone H3K27me3 enrichment at the *PFKP* promoter (K) in patient biopsies. Statistical significance was assessed using a Welch's *t* test with $P < .05$ considered significant. An ordinary 1-way ANOVA corrected for multiple comparisons using Tukey's method was used for Figure 2E and F. $^{**}P < .01$, $^{***}P < .005$, $^{****}P < .0001$.

Previous studies indicate that ATRX increases lysine 27 trimethylation of histone H3 (H3K27me3) at gene promoters,[9] resulting in transcriptional repression of gene expression.[39] ChIP-qRT-PCR indicated that ALT silencing via ATRX re-expression significantly increased histone H3K27me3 enrichment at the *PFKP* promoter in both BT257 and BT142 models (Figure 2G and H). In contrast, total histone H3 occupancy at the *PFKP* promoter was unaltered (Supplementary Figure S3H and I). These results suggest that ATRX negatively regulates PFKP expression via histone H3K27me3 deposition at the *PFKP* promoter and that ATRX loss in astrocytomas elevates *PFKP* expression and glycolytic flux.

To further confirm the clinical relevance of our findings, we examined biopsies from astrocytoma patients and compared with non-neoplastic gliosis biopsies, since procuring normal brain biopsies is not feasible.[28,30] We confirmed loss of ATRX and significantly elevated c-circles in astrocytoma biopsies relative to gliosis (Supplementary Figure S4A and B), in line with ALT-mediated telomere maintenance in astrocytomas. Importantly, PFKP mRNA and PFK activity were significantly higher while histone H3K27me3 enrichment at the *PFKP* promoter was significantly lower in astrocytoma biopsies relative to gliosis (Figure 2I–K), linking the ALT pathway to elevated PFK in clinically relevant patient biopsies.

## Glucose Flux to Lactate Is Reduced in ALT-Dependent Astrocytoma Cells Treated With the PARPi Niraparib

PARPi including the brain-penetrant niraparib induce DNA damage and lethal telomeric fusion in cells using the ALT pathway, thereby identifying a therapeutic opportunity for ALT-dependent tumors.[13,14,16] Since our results suggest that the ALT pathway is linked to higher glycolytic flux, we examined whether lactate production serves as a biomarker of response to niraparib in astrocytomas. First, we confirmed that niraparib significantly reduced cell viability in both $NHA_{ALT}$ and BT257 models (Figure 3A and B). Consistent with previous studies,[16] niraparib induced telomeric fusion as assessed by telomeric fluorescence in situ hybridization in the $NHA_{ALT}$ and BT257 models (Figure 3C–E). Importantly, PFK activity (Figure 3F and G) and [3-$^{13}$C]-lactate production from [1-$^{13}$C]-glucose (Figure 3H and I) were significantly reduced by niraparib in both $NHA_{ALT}$ and BT257 models.

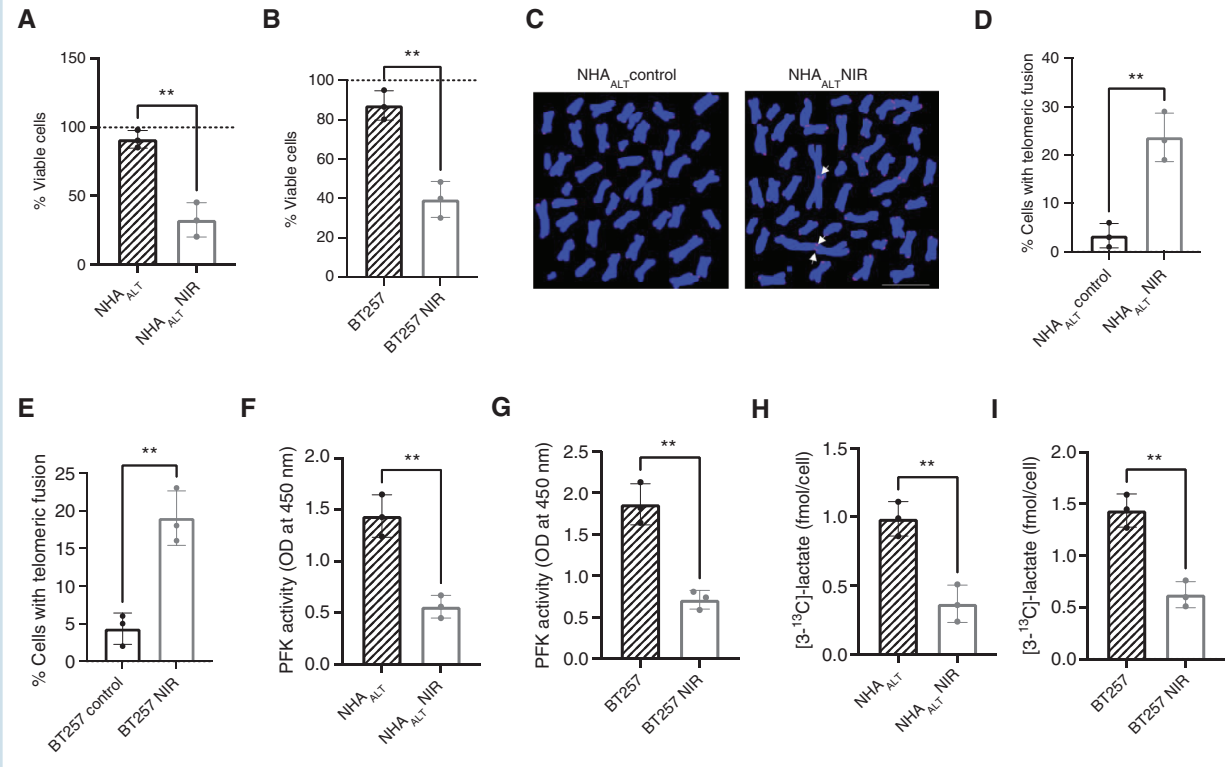


**Fig. 3** Niraparib reduces glycolytic flux in astrocytoma cells. Effect of niraparib on cell viability in the $NHA_{ALT}$ (A) and BT257 (B) models. (C) Representative images showing the effect of niraparib on telomeric fusion in the $NHA_{ALT}$ model. Scale bar is 10 μm. Quantification of the percentage of cells exhibiting telomeric fusion following niraparib treatment in the $NHA_{ALT}$ (D) and BT257 (E) models. Effect of niraparib on PFK activity in $NHA_{ALT}$ (F) and BT257 (G) cells. Effect of niraparib on [3-$^{13}$C]-lactate production from [1-$^{13}$C]-glucose in $NHA_{ALT}$ (H) and BT257 (I) cells. Statistical significance was assessed using a Welch's *t* test with $P < .05$ considered significant. $^{**}P < .01$.

## [6,6′-$^2$H]-Glucose Flux to Lactate Can Be Used to Monitor Tumor Burden in Mice-Bearing Orthotopic Astrocytomas In Vivo

$^2$H-MRS following administration of [6,6′-$^2$H]-glucose is a novel, clinically translatable method of imaging glucose metabolism in vivo.[23,24,35] Given the link between the ALT pathway and glycolysis, we examined whether $^2$H-MRS-based imaging of glucose metabolism serves to visualize tumor burden in ALT-dependent astrocytomas in vivo. Following intravenous injection of [6,6′-$^2$H]-glucose, non-localized acquisition of $^2$H-MR spectra showed dynamic production of lactate in mice bearing orthotopic $NHA_{ALT}$ tumors (Figure 4A). Since $NHA_{CONTROL}$ cells lack a telomere maintenance mechanism and do not form tumors in vivo, we examined tumor-free mice as controls. As shown in Supplementary Figure S5A, tumor-free normal brain produced high levels of glx and lower lactate from [6,6′-$^2$H]-glucose, consistent with previous studies.[23,25,35] These differences between tumor-bearing and tumor-free mice are highlighted in the summed $^2$H-spectra shown in Figure 4B. Quantification of the data confirmed significantly higher lactate concentration (Figure 4C) and normalized lactate (Supplementary Figure S5B) in $NHA_{ALT}$ tumor-bearing mice relative to tumor-free controls. Conversely, glx concentration and normalized glx levels were higher in the normal brain of tumor-free controls relative to $NHA_{ALT}$ tumor-bearing mice (Supplementary Figure S5C and D).

We obtained similar results in the patient-derived BT257 model. $^2$H-MR spectra acquired following [6,6′-$^2$H]-glucose injection into mice bearing orthotopic BT257 tumors showed higher lactate and lower glx relative to tumor-free controls (Figure 4D). Quantification of the results showed higher lactate concentration (Figure 4E) and normalized lactate (Supplementary Figure S5E) in BT257 tumor-bearing mice relative to tumor-free controls. In contrast, glx production was significantly reduced in BT257 tumor-bearing mice relative to tumor-free controls (Supplementary Figure S5F and G).

We then examined the spatial distribution of glucose metabolism in vivo using 2D CSI. Lactate production from [6,6′-$^2$H]-glucose was significantly higher in tumor relative to contralateral normal brain (Supplementary Figure

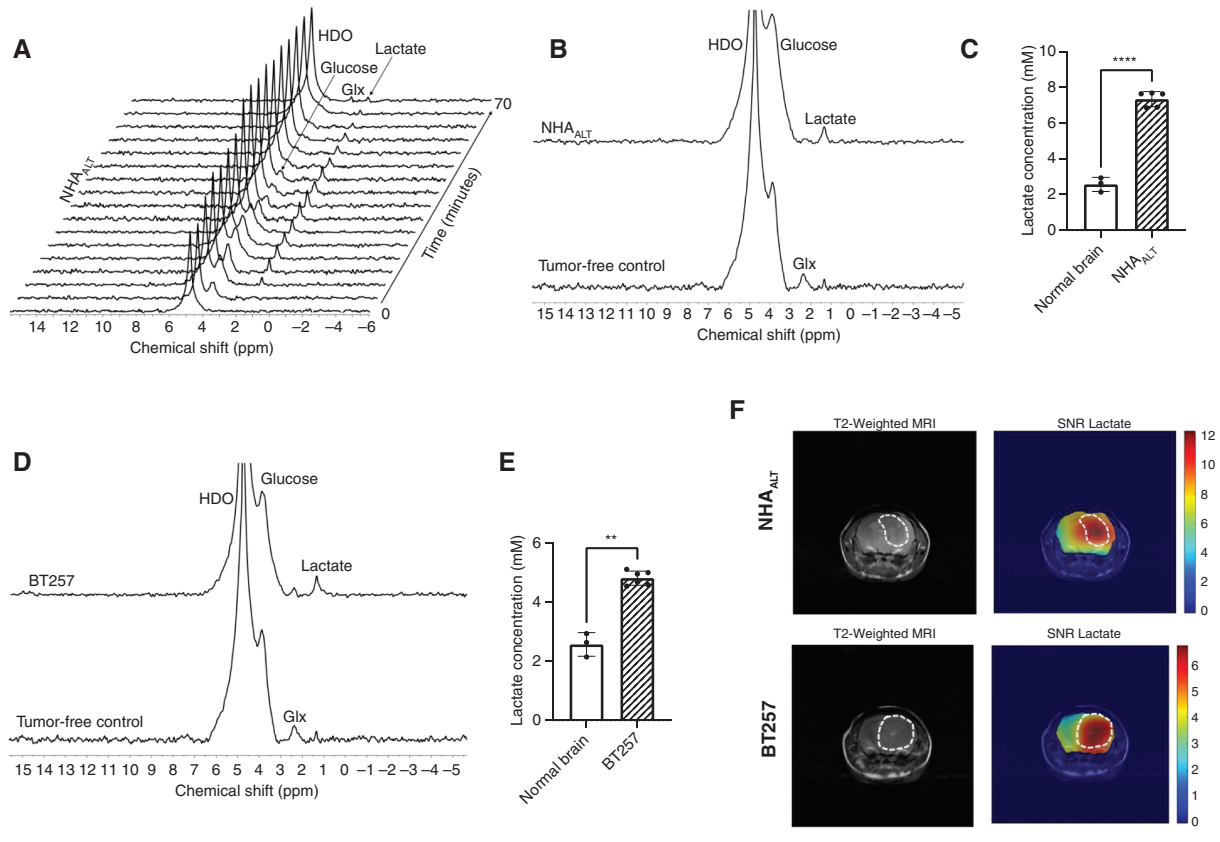


**Fig. 4** [6,6′-$^2$H]-glucose non-invasively monitors tumor burden in astrocytomas in vivo. (A) Representative $^2$H-MR spectral array of [6,6′-$^2$H]-glucose metabolism in a mouse bearing an orthotopic $NHA_{ALT}$ tumor. Peaks for glucose, lactate, glx, and HDO are labeled. Representative summed $^2$H-MR spectra (B, D) and lactate concentration (C, E) in mice bearing orthotopic $NHA_{ALT}$ or BT257 tumors or tumor-free controls. (F) Representative T2-weighted MRI (left) and heatmap of [3,3′-$^2$H]-lactate (right) from mice bearing $NHA_{ALT}$ (top panel) or BT257 (bottom panel) tumors. Tumor is contoured in white. Statistical significance was assessed using a Welch's *t* test with $P < .05$ considered significant. $^{**}P < .01$, $^{****}P < .0001$.

S6A and B), consistent with the non-localized $^{2}$H-MRS studies. The SNR of glx in the CSI studies was too low to allow reliable quantification (Supplementary Figure S6A). Importantly, visualization of the data as heatmaps showed that the [3,3′-$^{2}$H]-lactate signal demarcated tumor from contralateral normal brain in mice bearing orthotopic $NHA_{ALT}$ or BT257 tumors (Figure 4F). Collectively, these results indicate that monitoring ALT status using [6,6′-$^{2}$H]-glucose allows assessment of tumor burden in astrocytomas in vivo.

## Lactate Production From [6,6′-$^{2}$H]-Glucose Is an Early Biomarker of Response to Niraparib in Astrocytomas In Vivo

Next, we examined whether [6,6′-$^{2}$H]-glucose can be used to monitor astrocytoma response to therapy. Mice bearing orthotopic $NHA_{ALT}$ tumors were treated with vehicle-control or niraparib, and tumor volume was assessed by T2-weighted MRI. As shown in Figure 5A and B, niraparib induced MRI-detectable tumor shrinkage starting day 9 ± 2, an effect that was associated with significantly higher median survival (9 days for the vehicle-control group vs 75 days for the niraparib-treated group, $P < .005$). We then examined [6,6′-$^{2}$H]-glucose metabolism in vehicle-control and niraparib-treated mice at timepoints preceding MRI-detectable volumetric alterations (see representative T2-weighted MRI at days 0, 3, and 5 in Figure 5C). As shown in Figure 5D, there was no significant difference in [3,3′-$^{2}$H]-lactate concentration between vehicle-control and niraparib-treated $NHA_{ALT}$ tumor-bearing mice at day 0 (prior to the start of treatment). [3,3′-$^{2}$H]-lactate concentration significantly increased in vehicle-treated mice at day 3 and day 5 relative to day 0 (Figure 5D). In contrast, there was a significant reduction in [3,3′-$^{2}$H]-lactate concentration in niraparib-treated mice at day 3 and day 5 relative to day 0. Quantification of normalized lactate yielded similar results (Supplementary Figure S7A).

We obtained similar results with the patient-derived BT257 model. Niraparib induced tumor shrinkage starting day 18 ± 2 (Figure 6A) and significantly extended median survival (13 days for the vehicle-control group and 52 days

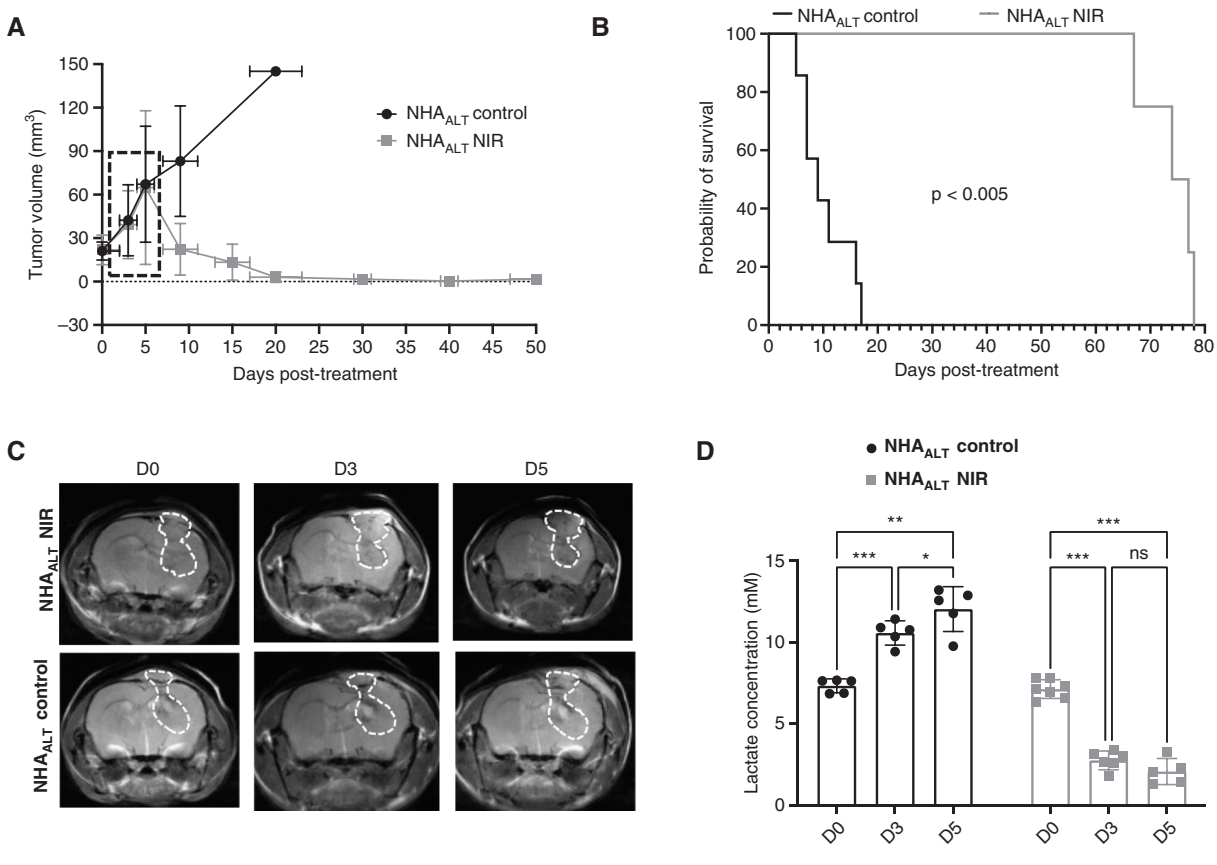


**Fig. 5** [6,6′-$^{2}$H]-glucose flux to lactate provides a readout of response to niraparib in vivo in the $NHA_{ALT}$ model. Tumor volume (A) and animal survival (B) in $NHA_{ALT}$ tumor-bearing mice treated with vehicle-control or niraparib. Dotted box highlights timepoints for $^{2}$H-MRS prior to the onset of tumor shrinkage. (C) Representative T2-weighted MRI at early timepoints (D0, D3, and D5) from vehicle-control or niraparib-treated $NHA_{ALT}$ tumor-bearing mice. (D) Lactate concentration in $NHA_{ALT}$ tumor-bearing mice treated with either vehicle-control or niraparib. Statistical significance was assessed using Kaplan-Meier survival analysis (Figure 2B) or an ordinary 2-way ANOVA corrected for multiple comparisons using Tukey's method (Figure 2D). *$P < .05$, **$P < .01$, ***$P < .005$, ns, not significant.

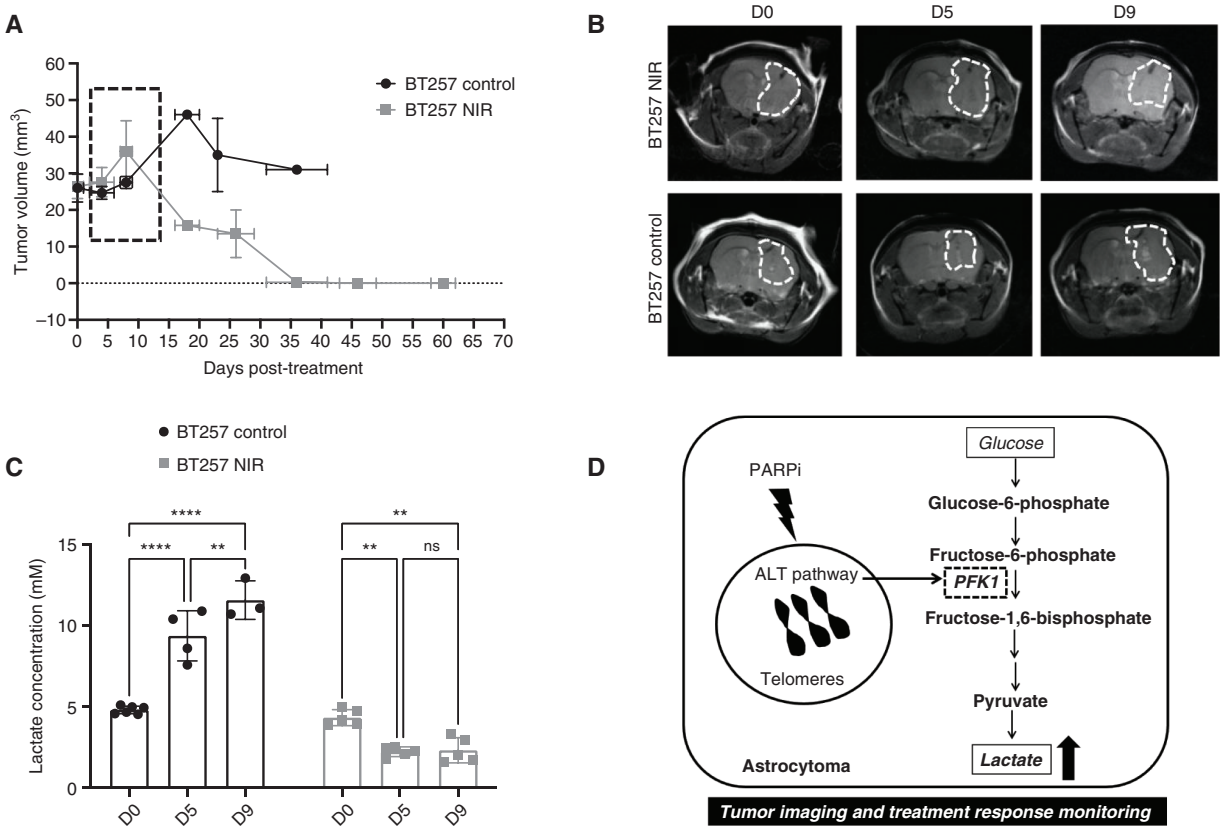


**Fig. 6** [6,6′-$^2$H]-glucose reports on early response to niraparib in the patient-derived BT257 model. (A) Tumor volume in BT257 tumor-bearing mice treated with vehicle-control or niraparib. Dotted box highlights timepoints for $^2$H-MRS prior to tumor shrinkage. (B) Representative T2-weighted MRI at early timepoints (D0, D5, and D9) from vehicle-control or niraparib-treated BT257 tumor-bearing mice. (C) Lactate concentration in mice bearing orthotopic BT257 tumors that were treated with vehicle-control or niraparib. (D) Schematic summary of our findings. The ALT pathway elevates glycolytic flux via PFK1. This metabolic reprogramming and response to PARPi that cause telomeric fusion in ALT cells can be non-invasively monitored via quantification of lactate production from [6,6′-$^2$H]-glucose. Statistical significance was assessed using an ordinary 2-way ANOVA corrected for multiple comparisons using Tukey's method. $^{**}P < .01$, $^{****}P < .0001$, ns, not significant.

for the niraparib-treated group, $P < .005$; Supplementary Figure S7B). Importantly, [3,3′-$^2$H]-lactate concentration significantly dropped in niraparib-treated mice at day 5 and day 9 post-treatment, when tumor volume was unaltered on T2-weighted MRI (Figure 6B and C). In contrast, [3,3′-$^2$H]-lactate concentration significantly increased at day 5 and day 9 relative to day 0 in vehicle-treated mice (Figure 6C). Quantification of normalized lactate provided similar results (Supplementary Figure S7C). Niraparib did not alter glx production from [6,6′-$^2$H]-glucose for either the $NHA_{ALT}$ or BT257 model (Supplementary Figure S7D and E), ruling out glx as a biomarker of treatment response. Collectively, these results validate lactate production from [6,6′-$^2$H]-glucose as an early biomarker of response to niraparib and, importantly, point to the potential of [6,6′-$^2$H]-glucose for imaging pseudoprogression in vivo.

## Discussion

The ALT pathway plays a key role in tumor proliferation in astrocytomas.[2,5,7] In this study, we used isogenic pairs of cell lines that differed only in their ALT status, including both genetically engineered and patient-derived models, to link the ALT pathway to elevated glycolytic flux via PFK1. Importantly, we leveraged this information for noninvasive $^2$H-MRS-based imaging of tumor burden and response to therapy in vivo (see schematic summary in Figure 6D).

To the best of our knowledge, our study is the first to link the ALT pathway with PFK1. ALT silencing via ATRX re-expression downregulates PFKP expression and activity as well as glucose flux to lactate in patient-derived astrocytoma models. Conversely, PFKP overexpression in ALT- neurospheres rescues glycolytic flux, pointing to the causal role of PFK1 in the ALT-linked upregulation of glycolytic flux in astrocytomas. Mechanistically, ATRX re-expression downregulates *PFKP* by increasing histone H3K27me3 enrichment, which is associated with repression of gene transcription,[39] at the *PFKP* promoter. Importantly, histone H3K27me3 deposition at the *PFKP* promoter is reduced and PFKP expression concomitantly elevated in astrocytoma biopsies relative to non-neoplastic gliosis biopsies, pointing to the clinical relevance of our results. In essence, our study suggests that ATRX loss simultaneously drives the development of the ALT pathway and

the elevation of glycolytic flux via PFK1, thereby identifying a mechanistic link between telomere maintenance and elevated glycolysis.

We previously showed that $^{1}$H-MRS-detectable α-ketoglutarate is elevated in ALT cells.[28] Since α-ketoglutarate plays a role in the conversion of alanine to pyruvate, we leveraged this metabolic reprogramming for noninvasive imaging of astrocytomas using hyperpolarized [1-$^{13}$C]-alanine.[28] In a separate study focused on imaging telomerase reverse transcriptase, which is the telomere maintenance mechanism in IDHmut oligodendrogliomas, we examined the $NHA_{ALT}$ model as a negative control and showed that hyperpolarized [U-$^{13}$C, U-$^{2}$H]-glucose is metabolized to lactate in $NHA_{ALT}$ cells.[26] In the current study, we have established that glycolytic flux is, indeed, elevated in ALT cells and mechanistically validated [6,6′-$^{2}$H]-glucose as a complementary probe for imaging the ALT pathway. To date, $^{2}$H-MRS studies of [6,6′-$^{2}$H]-glucose have focused on glioblastomas and lymphomas.[23,24] Our study, for the first time, highlights the utility of [6,6′-$^{2}$H]-glucose for imaging IDHmut astrocytomas. Importantly, our results can be rapidly translated to the clinic since the feasibility of imaging tumor burden using [6,6′-$^{2}$H]-glucose has been established in glioblastoma patients.[23] Furthermore, although our studies were conducted at 14.1T, $^{2}$H-MRS has been performed at the clinically relevant field strength of 4T in glioblastoma patients,[23] underscoring the clinical translatability of our results.

Previous studies suggest that promoter hypermethylation downregulates expression of lactate dehydrogenase A (LDHA), the enzyme that converts pyruvate to lactate, resulting in a lack of difference in LDHA expression[40,41] and steady-state lactate[42] between IDHmut gliomas and normal brain in preclinical models. As a result, IDHmut gliomas are considered non-glycolytic tumors.[40–42] However, our studies indicate that elevated PFK activity, which is upstream of LDHA, increases glucose flux to lactate to levels sufficient to discriminate astrocytoma cells from normal astrocytes and, importantly, to levels that enable noninvasive [6,6′-$^{2}$H]-glucose-based discrimination of astrocytoma tumors from the normal brain. These results are consistent with recent studies indicating that glycolytic flux is controlled at a few steps whose upregulation underlies the Warburg effect, including hexokinase and PFK1, but not LDHA.[37] Our study also highlights the utility of monitoring glucose flux to lactate, as opposed to assessing steady-state lactate, for astrocytoma imaging.

$^{2}$H-MRS provides information that is complementary to hyperpolarized $^{13}$C-MRS. Previous studies have established the ability of hyperpolarized $^{13}$C-MRS to report on dynamic lactate production in vivo.[22] Depending on the design of the study, lactate production from [6,6′-$^{2}$H]-glucose can be examined at isotopic steady-state[23] or in a dynamic manner as shown previously[25] and in our studies with the $NHA_{ALT}$ model. Importantly, by tracing flux through metabolic pathways such as glycolysis in vivo, both $^{2}$H- and hyperpolarized $^{13}$C-MRS provide information on metabolic pathway activity that has hitherto been inaccessible in a noninvasive manner. One point of difference between the 2 methods is the timing of information capture. Unlike hyperpolarized $^{13}$C-MRS which assesses metabolic fluxes within a short time (<5 minutes),[22] $^{2}$H-MRS provides a readout of metabolic flux over a longer window (30-60 minutes). One possible consequence of this difference is the ability to observe tricarboxylic acid cycle-mediated flux of [6,6′-$^{2}$H]-glucose to glx, while we[26] and others[43–45] have been unable to observe glx production from hyperpolarized [U-$^{13}$C, U-$^{2}$H]-glucose. Another difference is the higher concentration of [6,6′-$^{2}$H]-glucose used in our study (1 g/kg), which is twice the hyperpolarized [U-$^{13}$C, U-$^{2}$H]-glucose concentration used previously.[26] Nevertheless, the concentration of 1 g/kg for [6,6′-$^{2}$H]-glucose is lower than the concentration used in previous $^{2}$H-MRS studies[23–25,35] and, importantly, did not lead to any adverse events. Finally, with regard to clinical translation, $^{2}$H-MRS provides a technically simpler and lower-cost method of imaging the ALT pathway, requiring primarily the acquisition of a radiofrequency coil as opposed to a hyperpolarizer, which could aid in dissemination and widespread application to astrocytoma imaging.[23]

Our study, to the best of our knowledge for the first time, demonstrates the utility of [6,6′-$^{2}$H]-glucose for imaging pseudoprogression in astrocytomas in vivo. Pseudoprogression occurs following treatment with chemotherapy, radiotherapy, or targeted inhibitors and manifests as a lesion that cannot be distinguished from tumor by conventional MRI.[46] The inability to assess pseudoprogression results in incorrect treatment with devastating consequences and hampers evaluation of the efficacy of inhibitors in clinical trials. Our results show that, following niraparib treatment, [6,6′-$^{2}$H]-glucose flux to lactate is reduced at early timepoints preceding MRI-detectable alterations, thereby enabling visualization of pseudoprogression in vivo. By allowing assessment of early response, $^{2}$H-MRS-based imaging of the ALT pathway can also aid in clinical translation of PARPi. Further studies are needed to determine whether [6,6′-$^{2}$H]-glucose reports on response to other ALT inhibitors such as berzosertib[15] and to standard of care radiochemotherapy.

In summary, we have linked the ALT pathway to elevated glycolytic flux via PFK1 and identified [6,6′-$^{2}$H]-glucose as a novel agent for metabolic imaging of the ALT pathway in astrocytomas in vivo. Our study has the potential to significantly impact the longitudinal imaging of tumor burden and response to therapy in astrocytoma patients.

## Supplementary Material

Supplementary material is available at *Neuro-Oncology* online.

## Keywords

alternative lengthening of telomeres | astrocytomas | deuterium metabolic imaging | gliomas | isocitrate dehydrogenase mutation

## Funding

This work was funded by the National Institutes of Health (NIH R01CA239288), Department of Defense (W81XWH201055315), UCSF NICO, and Loglio. The authors also acknowledge support from NIH P01CA118816, R01CA172845, R01CA197254, and R01NS105087.

**Conflict of interest statement.** The authors have no conflicting interests to disclose.

**Authorship statement.** P.V. conceptualized the research; P.V., C.T., G.B., J.M., and M.T. performed and analyzed the experiments; A.M.G. and D.H. assisted with cell and in vivo studies; H.A.L. and R.O.P. provided cell lines and reagents; P.V. and C.T. wrote the manuscript; P.V., C.T., G.B., and H.A.L. reviewed the manuscript; P.V., S.M.R., and R.O.P. contributed to funding.

## References

1. Shay JW, Wright WE. Telomeres and telomerase: three decades of progress. *Nat Rev Genet.* 2019;20(5):299–309.
2. Dilley RL, Greenberg RA. ALTernative telomere maintenance and cancer. *Trends Cancer.* 2015;1(2):145–156.
3. Danussi C, Bose P, Parthasarathy PT, et al. *Atrx* inactivation drives disease-defining phenotypes in glioma cells of origin through global epigenomic remodeling. *Nat Commun.* 2018;9(1):1057.
4. Clynes D, Jelinska C, Xella B, et al. Suppression of the alternative lengthening of telomere pathway by the chromatin remodelling factor ATRX. *Nat Commun.* 2015;6:7538.
5. Sieverling L, Hong C, Koser SD, et al. Genomic footprints of activated telomere maintenance mechanisms in cancer. *Nat Commun.* 2020;11(1):733.
6. Mukherjee J, Johannessen TC, Ohba S, et al. Mutant IDH1 cooperates with ATRX loss to drive the alternative lengthening of telomere phenotype in glioma. *Cancer Res.* 2018;78(11):2966–2977.
7. Ferreira MSV, Sørensen MD, Pusch S, et al. Alternative lengthening of telomeres is the major telomere maintenance mechanism in astrocytoma with isocitrate dehydrogenase 1 mutation. *J Neurooncol.* 2020;147(1):1–14.
8. Wiestler B, Capper D, Holland-Letz T, et al. ATRX loss refines the classification of anaplastic gliomas and identifies a subgroup of *IDH* mutant astrocytic tumors with better prognosis. *Acta Neuropathol.* 2013;126(3):443–451.
9. Haase S, Garcia-Fabiani MB, Carney S, et al. Mutant ATRX: uncovering a new therapeutic target for glioma. *Expert Opin Ther Targets.* 2018;22(7):599–613.
10. Louis DN, Perry A, Wesseling P, et al. The 2021 WHO classification of tumors of the central nervous system: a summary. *Neuro Oncol.* 2021;23(8):1231–1251.
11. Jiao Y, Killela PJ, Reitman ZJ, et al. Frequent ATRX, CIC, FUBP1 and IDH1 mutations refine the classification of malignant gliomas. *Oncotarget* 2012;3(7):709–722.
12. Ebrahimi A, Skardelly M, Bonzheim I, et al. ATRX immunostaining predicts IDH and H3F3A status in gliomas. *Acta Neuropathol Commun.* 2016;4(1):60.
13. Garbarino J, Eckroate J, Sundaram RK, Jensen RB, Bindra RS. Loss of ATRX confers DNA repair defects and PARP inhibitor sensitivity. *Transl Oncol.* 2021;14(9):101147.
14. Sule A, Van Doorn J, Sundaram RK, Ganesa S, Vasquez JC, Bindra RS. Targeting IDH1/2 mutant cancers with combinations of ATR and PARP inhibitors. *NAR Cancer.* 2021;3(2):zcab018.
15. Flynn RL, Cox KE, Jeitany M, et al. Alternative lengthening of telomeres renders cancer cells hypersensitive to ATR inhibitors. *Science.* 2015;347(6219):273–277.
16. Mukherjee J, Pandita A, Kamalakar C, et al. A subset of PARP inhibitors induces lethal telomere fusion in ALT-dependent tumor cells. *Sci Transl Med.* 2021;13(592):eabc7211.
17. Lal S, Snape TJ. A therapeutic update on PARP inhibitors: implications in the treatment of glioma. *Drug Discov Today.* 2021;26(2):532–541.
18. Henson JD, Cao Y, Huschtscha LI, et al. DNA C-circles are specific and quantifiable markers of alternative-lengthening-of-telomeres activity. *Nat Biotechnol.* 2009;27(12):1181–1185.
19. Lau LM, Dagg RA, Henson JD, Au AY, Royds JA, Reddel RR. Detection of alternative lengthening of telomeres by telomere quantitative PCR. *Nucleic Acids Res.* 2013;41(2):e34.
20. Ruiz-Rodado V, Brender JR, Cherukuri MK, Gilbert MR, Larion M. Magnetic resonance spectroscopy for the study of CNS malignancies. *Prog Nucl Magn Reson Spectrosc.* 2021;122:23–41.
21. Wijnen JP, Van der Graaf M, Scheenen TW, et al. In vivo $^{13}$C magnetic resonance spectroscopy of a human brain tumor after application of $^{13}$C-1-enriched glucose. *Magn Reson Imaging.* 2010;28(5):690–697.
22. Viswanath P, Li Y, Ronen SM. C-13 Hyperpolarized MR spectroscopy for metabolic imaging of brain tumors. In: Pope WB, ed. *Glioma Imaging: Physiologic, Metabolic, and Molecular Approaches.* Cham, Switzerland: Springer International Publishing; 2020:191–209.
23. De Feyter HM, Behar KL, Corbin ZA, et al. Deuterium metabolic imaging (DMI) for MRI-based 3D mapping of metabolism in vivo. *Sci Adv.* 2018;4(8):eaat7314.
24. Kreis F, Wright AJ, Hesse F, Fala M, Hu DE, Brindle KM. Measuring tumor glycolytic flux in vivo by using fast deuterium MRI. *Radiology.* 2020;294(2):289–296.
25. Lu M, Zhu XH, Zhang Y, Mateescu G, Chen W. Quantitative assessment of brain glucose metabolic rates using in vivo deuterium magnetic resonance spectroscopy. *J Cereb Blood Flow Metab.* 2017;37(11):3518–3530.
26. Viswanath P, Batsios G, Ayyappan V, et al. Metabolic imaging detects elevated glucose flux through the pentose phosphate pathway associated with TERT expression in low-grade gliomas. *Neuro Oncol.* 2021;23(9):1509–1522.
27. Ohba S, Mukherjee J, Johannessen TC, et al. Mutant IDH1 expression drives *TERT* promoter reactivation as part of the cellular transformation process. *Cancer Res.* 2016;76(22):6680–6689.
28. Viswanath P, Batsios G, Mukherjee J, et al. Non-invasive assessment of telomere maintenance mechanisms in brain tumors. *Nat Commun.* 2021;12(1):92.
29. Luchman HA, Stechishin OD, Dang NH, et al. An in vivo patient-derived model of endogenous IDH1-mutant glioma. *Neuro Oncol.* 2012;14(2):184–191.
30. Luchman HA, Chesnelong C, Cairncross JG, Weiss S. Spontaneous loss of heterozygosity leading to homozygous R132H in a patient-derived *IDH1* mutant cell line. *Neuro Oncol.* 2013;15(8):979–980.
31. Mazor T, Chesnelong C, Pankov A, et al. Clonal expansion and epigenetic reprogramming following deletion or amplification of mutant *IDH1*. *Proc Natl Acad Sci USA.* 2017;114(40):10743–10748.

32. Jensen KV, Cseh O, Aman A, Weiss S, Luchman HA. The JAK2/STAT3 inhibitor pacritinib effectively inhibits patient-derived GBM brain tumor initiating cells *in vitro* and when used in combination with temozolomide increases survival in an orthotopic xenograft model. *PLoS One*. 2017;12(12):e0189670.
33. Viswanath P, Radoul M, Izquierdo-Garcia JL, et al. Mutant IDH1 gliomas downregulate phosphocholine and phosphoethanolamine synthesis in a 2-hydroxyglutarate-dependent manner. *Cancer Metab*. 2018;6:3.
34. Viswanath P, Radoul M, Izquierdo-Garcia JL, et al. 2-Hydroxyglutarate-mediated autophagy of the endoplasmic reticulum leads to an unusual downregulation of phospholipid biosynthesis in mutant IDH1 gliomas. *Cancer Res*. 2018;78(9):2290–2304.
35. Rich LJ, Bagga P, Wilson NE, et al. $^{1}$H magnetic resonance spectroscopy of $^{2}$H-to-$^{1}$H exchange quantifies the dynamics of cellular metabolism in vivo. *Nat Biomed Eng*. 2020;4(3):335–342.
36. Glunde K, Bhujwalla ZM, Ronen SM. Choline metabolism in malignant transformation. *Nat Rev Cancer*. 2011;11(12):835–848.
37. Tanner LB, Goglia AG, Wei MH, et al. Four key steps control glycolytic flux in mammalian cells. *Cell Syst*. 2018;7(1):49–62.e8.
38. Lee JH, Liu R, Li J, et al. Stabilization of phosphofructokinase 1 platelet isoform by AKT promotes tumorigenesis. *Nat Commun*. 2017;8(1):949.
39. Blackledge NP, Klose RJ. The molecular principles of gene regulation by Polycomb repressive complexes. *Nat Rev Mol Cell Biol*. 2021;22(12):815–833.
40. Chesnelong C, Chaumeil MM, Blough MD, et al. Lactate dehydrogenase A silencing in IDH mutant gliomas. *Neuro Oncol*. 2014;16(5):686–695.
41. Victor RR, Malta TM, Seki T, et al. Metabolic reprogramming associated with aggressiveness occurs in the G-CIMP-high molecular subtypes of IDH1*mut* lower grade gliomas. *Neuro Oncol*. 2019;22(4):480–492.
42. Ruiz-Rodado V, Seki T, Dowdy T, et al. Metabolic landscape of a genetically engineered mouse model of IDH1 mutant glioma. *Cancers (Basel)*. 2020;12(6):1633.
43. Rodrigues TB, Serrao EM, Kennedy BW, Hu DE, Kettunen MI, Brindle KM. Magnetic resonance imaging of tumor glycolysis using hyperpolarized 13C-labeled glucose. *Nat Med*. 2014;20(1):93–97.
44. Harris T, Degani H, Frydman L. Hyperpolarized $^{13}$C NMR studies of glucose metabolism in living breast cancer cell cultures. *NMR Biomed*. 2013;26(12):1831–1843.
45. Mishkovsky M, Gusyatiner O, Lanz B, et al. Hyperpolarized $^{13}$C-glucose magnetic resonance highlights reduced aerobic glycolysis in vivo in infiltrative glioblastoma. *Sci Rep*. 2021;11(1):5771.
46. Hygino da Cruz LC, Rodriguez I, Domingues RC, Gasparetto EL, Sorensen AG. Pseudoprogression and pseudoresponse: imaging challenges in the assessment of posttreatment glioma. *Am J Neuroradiol*. 2011;32(11):1978.